Journal of Materials Chemistry

Cite this: *J. Mater. Chem.*, 2012, **22**, 10221

www.rsc.org/materials

PAPER

Mixed gas adsorption of carbon dioxide and methane on a series of isoreticular microporous metal–organic frameworks based on 2-substituted imidazolate-4-amide-5-imidates†

Franziska Debatin,[a] Jens Möllmer,[b] Suvendu Sekhar Mondal,[a] Karsten Behrens,[a] Andreas Möller,[b] Reiner Staudt,*[c] Arne Thomas[d] and Hans-Jürgen Holdt*[a]

Received 11th November 2011, Accepted 6th January 2012
DOI: 10.1039/c2jm15811f

In this work the adsorption of CO_2 and CH_4 on a series of isoreticular microporous metal–organic frameworks based on 2-substituted imidazolate-4-amide-5-imidates, **IFP-1–IFP-6** (**IFP** = Imidazolate Framework Potsdam), is studied firstly by pure gas adsorption at 273 K. All experimental isotherms can be nicely described by using the Tòth isotherm model and show the preferred adsorption of CO_2 over CH_4. At low pressures the Tòth isotherm equation exhibits a Henry region, wherefore Henry's law constants for CO_2 and CH_4 uptake could be determined and ideal selectivity α_{CO_2/CH_4} has been calculated. Secondly, selectivities were calculated from mixture data by using nearly equimolar binary mixtures of both gases by a volumetric–chromatographic method to examine the **IFPs**. Results showed the reliability of the selectivity calculation. Values of α_{CO_2/CH_4} around 7.5 for **IFP-5** indicate that this material shows much better selectivities than **IFP-1**, **IFP-2**, **IFP-3**, **IFP-4** and **IFP-6** with slightly lower selectivity $\alpha_{CO_2/CH_4} = 4–6$. The preferred adsorption of CO_2 over CH_4 especially of **IFP-5** and **IFP-4** makes these materials suitable for gas separation application.

1 Introduction

Recently we synthesized a new series of isoreticular metal–organic frameworks, **IFP-1**,[1] **IFP-2**,[2] **IFP-3**,[2] **IFP-4**,[2] **IFP-5**[3] and **IFP-6**,[3] based on 2-substituted imidazolate-4-amide-5-imidates (Scheme 1). The 2-substituted imidazolate-4-amide-5-imidates, **1a–1d** {**1a** (R = methyl), **1b** (R = chloro), **1c** (R = bromo), **1d** (R = ethyl)}, link with the metal ions (**IFP-1–IFP-4**: Zn^{2+}, **IFP-5**: Co^{2+}, **IFP-6**: Cd^{2+}) and form neutral microporous imidazolate metal–organic frameworks with 1D hexagonal channels. The chelate ligands **1a–1d** show a strong structure-directing effect: the combination of amide/imidate and imidazolate groups causes a strong tendency for coordination and generates a permanent porosity in the **IFP**s. The rigidity and stability of **1a–1d** also impart excellent thermal and water stability to the **IFP**s. Moreover, the imidazolate-amide-imidate linkers polarize the walls of the microporous channels. The 2-substituent R of the linkers **1a–1d** protrudes into the open channels (Scheme 1). For this

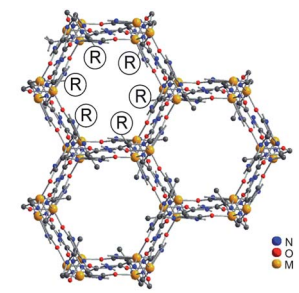

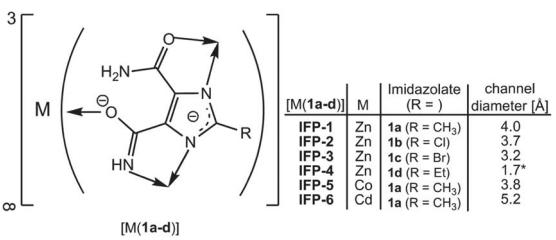

[M(1a-d)]	M	Imidazolate (R =)	channel diameter [Å]
IFP-1	Zn	1a (R = CH_3)	4.0
IFP-2	Zn	1b (R = Cl)	3.7
IFP-3	Zn	1c (R = Br)	3.2
IFP-4	Zn	1d (R = Et)	1.7*
IFP-5	Co	1a (R = CH_3)	3.8
IFP-6	Cd	1a (R = CH_3)	5.2

Scheme 1 A sketch of the 1D hexagonal channels in a series of isoreticular Imidazolate Framework Potsdam **IFP-1** to **IFP-6** (*channel diameter based on density functional *ab initio* calculation).

[a]*Institut für Chemie, Anorganische Chemie, Universität Potsdam, 14476 Potsdam, Germany. E-mail: holdt@uni-potsdam.de; Fax: +49 331 977-5055; Tel: +49 331 977-5180*
[b]*Institut für Nichtklassische Chemie e.V., Universiät Leipzig, 04318 Leipzig, Germany. E-mail: moeller@inc.uni-leipzig.de; Fax: +49 341 2352-701; Tel: +49 341 2352-445*
[c]*Fakultät Maschinenbau und Verfahrenstechnik, Hochschule Offenburg, 77652 Offenburg, Germany. E-mail: reiner.staudt@fh-offenburg.de; Fax: +49 781 205-111; Tel: +49 781 205-161*
[d]*Institut für Chemie, Fakultät II, Technische Universität Berlin, 10623 Berlin, Germany. E-mail: arne.thomas@tu-berlin.de; Fax: +49 30 314-29271; Tel: +49 30 314-25118*

† Electronic supplementary information (ESI) available: Indicating spreading pressure diagrams of **IFP-1** to **IFP-6** at 273 K. See DOI: 10.1039/c2jm15811f

reason the accessible diameter and the functionality of the hexagonal channel in an **IFP** can be tuned by varying R. Furthermore the radius of the metal ion defines the channel diameter of an **IFP**. The accessible diameters of the channels in the **IFP**s are in the range of 1.7 to 5.2 Å (Scheme 1). In opposite to the tetrahedral coordination of the metal ions in well known **ZIF**s,[4] the metal ion in an **IFP** is pentacoordinated by the imidazolate-amide-imidate linkers to form a distorted environment with a trigonal-bipyramidal character. That means the **IFP** surface bears exposed metal centers. These can dramatically enhance (selective) gas uptake or serve as a source of catalytic activity. The **IFP**s, **IFP-1** to **IFP-4**, have significant capacity for the capture of CO_2 and a lower uptake capacity for CH_4.[1,2] In general higher uptakes of CO_2 in comparison to CH_4 are justified firstly by the quadrupole moment of CO_2 that could interact with the polar amide, imidate and imidazolate groups in the pore walls as well as with the exposed Zn^{2+} centers provided by **IFP-1** to **IFP-4**. Secondly the higher uptake is justified by the smaller kinetic diameter of CO_2 (3.3 Å) in comparison to CH_4 (3.8 Å).

2 Experimental

2.1 Pure gas adsorption studies

High pressure adsorption measurements of CO_2, CH_4 and He were performed on a magnetic suspension balance (Rubotherm, Germany). Various pressure transducers (MKS Baratron, US and Newport Omega, USA) were used in a range from vacuum up to 5 MPa with an accuracy of 0.05%.

In a typical experiment, a stainless steel sample holder was filled with about 500 mg of **IFP** material and the balance was evacuated for 12 hours at 473 K and 0.3 Pa until constant mass was achieved. For measuring the sorption capacity, the gas was dosed into the balance at elevated pressures. Equilibrium was achieved when no further weight increase was observed by microbalance within 15 minutes. In the case of CO_2, for **IFP-1**, **IFP-2**, **IFP-3**, **IFP-4** and **IFP-5** equilibrium was reached in 1 hour. In contrast, for CH_4 adsorption on **IFP-4** the equilibrium time was set to 10 hours. In the case of **IFP-6** for CO_2 and CH_4 adsorption, a equilibrium time of more than 16 hours was necessary. The temperature was kept constant with an accuracy of ±0.5 K in each measuring run.

Additionally, for each isotherm, a buoyancy correction with He as the probe gas was used to calculate the surface excess mass from the measured values. A detailed description of this procedure can be found elsewhere.[5] For the determination of the density from pressure and temperature, the program *FLUIDCAL* (Ruhr University Bochum, Germany) was used for each gas.[6]

2.2 Mixed gas adsorption studies

Binary adsorption measurements were performed on a self-made volumetric-chromatographic set-up. This set-up can be used for multi-component adsorption equilibria measurements. The overall pressure limit is 15 MPa within a temperature range of 263 to 353 K. The volume of the set-up was calculated by N_2 and Ar expansion experiments up to 15 MPa with and without a vessel filled by copper as the reference material. For binary adsorption measurement, at least 500 mg of **IFP** material was used for each experiment. Before the experiment, the sample was added into the sample cell and outgassed at 180 °C for 12 hours in a vacuum. The weight loss during activation was known from several gravimetric measurements. Nevertheless, for each **IFP** a pure gas isotherm for CO_2 and CH_4 was measured volumetrically and compared to gravimetric measured isotherms. The equilibrium time was carried out at a constant pressure value during the experiment, as well as by taking into consideration the adsorption kinetic from the gravimetric pure gas adsorption measurements. Depending on the knowledge of kinetics of pure gas adsorption for **IFP-4** and **IFP-6**, the mixture adsorption equilibrium time was set to more than 70 hours for both. For **IFP-1**, **IFP-2**, **IFP-3** and **IFP-5** the equilibrium time was set to 24 hours.

Based on a mass balance that includes the knowledge of vessel volume, pressure, temperature and gas phase concentration, the adsorbed amount can be calculated. The surface excess can further be determined by choosing the sample volume from gravimetric measured He isotherms.

In addition, different pressure transducers (Newport Omega, USA) were used in a range from vacuum up to 5 MPa with an accuracy of 0.05%. The temperature was kept constant with an accuracy of ±0.1 K. The gas phase concentration was analyzed offline using a Chrompack GC CP9001 (separation column: CarboPlot (25 m × 0.53 mm)) and Ar as the carrier gas by a thermal conductivity detector. Therefore, the gas phase was transferred to a sampling system, so that 100 μL of the gas mixture can be taken by a gas-tight syringe and furthermore transferred to the GC.

For the determination of the density from pressure, temperature and gas phase concentration, a calculation tool was used, which includes the equation of state based on GERG.[7]

A detailed procedure of binary adsorption measurement using this set-up as well as a schematic view of the system and a reference experiment using a well known activated carbon is given in ref. 8.

3 Theoretical section

Based on the simple Langmuir equation,[9,10] a model is used, which can describe pure gas adsorption isotherms in a wide range of pressure. The Tòth isotherm equation (eqn (1)) is a good description for this purpose and, as an advantage, this equation is a thermodynamically correct isotherm equation

$$\Theta = \frac{n^{\sigma}}{n_{\infty}^{\sigma}} = \frac{bp}{\left(1 + (bp)^{t}\right)^{1/t}} \quad (1)$$

(n^{σ}—adsorbed amount, $n_{\infty}{}^{\sigma}$—maximum adsorbed amount, b—the Tòth isotherm constant, and t—parameter related to the heterogeneity of the surface[9,11]).

At low pressures the Tòth isotherm equation exhibits a Henry region, where one can estimate the Henry's law constant, which is given by

$$H = bn_{\infty}^{\sigma} \quad (2)$$

By applying a fitting procedure of each isotherm, the average relative derivation between the experimental and modeled isotherm point was used for each isotherm by

$$\overline{\Delta}n^{\sigma} = \frac{100}{N}\sum_{i=1}^{N}\left|\frac{(n^{\sigma}_{\mathrm{exp}} - n_{\mathrm{mod}})}{n^{\sigma}_{\mathrm{exp}}}\right| \quad (3)$$

(N—the number of isotherm points, $n_{\mathrm{exp}}{}^{\sigma}$—experimental, and n_{mod}—modeled isotherm point).

The ideal adsorbed solution theory (IAST) was used for the prediction of multi-component adsorption equilibria.[12,13] The theory is based on an ideal adsorbed phase, where no interaction between the adsorbed molecules takes place. Analogous to Raoult's law, equilibria conditions can be described by

$$y_i p = p_i^0(\pi_i^0)x_i \quad (4)$$

(p—pressure, y_i—gas phase concentration of component i, x_i—adsorbed phase concentration of component i and p_i^0—equilibrium pressure for pure component i).

P_i^0 corresponds to the reduced spreading pressure of the mixture. The reduced spreading pressure can be expressed as

$$\frac{\pi A}{RT} = \int_0^p n(p)d\ln p \quad (5)$$

and calculated by using the Tòth isotherm model for pure gas adsorption isotherms. The spreading pressure can then be obtained for pure component i at a given y and p. By assuming a constant spreading pressure for each component

$$\pi_i^0 = \pi_j^0 = \ldots = \pi_n^0 \quad (6)$$

the adsorbed phase concentration x_i can be calculated. Furthermore, the Lewis rule makes it possible to evaluate the adsorbed amount of all components

$$\frac{1}{n^{\sigma}} = \sum_i \frac{x_i}{n_i^0}. \quad (7)$$

With the gas phase and adsorbed phase molar fraction from the binary adsorption measurements or from IAST prediction, the adsorption selectivity α for the components i and j is given as:[14]

$$\alpha_{i,j} = \left(\frac{x_i}{y_i}\right)\Big/\left(\frac{x_j}{y_j}\right) \quad (8)$$

In contrast, a value for selectivity can also be given from the pure gas adsorption isotherm. As followed by thermodynamics, the adsorption selectivity from expression (8) can be rearranged by the formulation of the Henry law to be

$$\lim_{p\to 0}\alpha_i = \left(\frac{n_i}{y_i}\right)\Big/\left(\frac{n_j}{y_j}\right) = \frac{H_i}{H_j}. \quad (9)$$

The selectivity derived by the Henry's law constants is a limit case and is valid for zero coverage of the solid surface.

4 Results and discussion

4.1 Adsorbent characterization

As already discussed in a previous work,[2] N_2 adsorption is not the most appropriate method to characterize the textural properties of porous materials with narrow micropores. As in the case of **IFP-1** to **IFP-4** better results are observed by measuring CO_2 adsorption at 273 K.[2] Therefore, CO_2 adsorption at 273 K was used to characterize the textural properties of all **IFP** materials in this study. By applying the BET method for microporous material[15] to the CO_2 adsorption isotherms (cross-sectional area of CO_2 to be 0.21 nm^2), the calculated BET surface areas decrease in the range **IFP-1** > **IFP-6** > **IFP-2** > **IFP-4** > **IFP-3** > **IFP-5** (Table 1). This ordering correlates especially in the case of **IFP-6** and **IFP-4** not with the range of decreasing effective channel diameters as shown in Scheme 1. We assume that activated **IFP-6** contains smaller channels (3–4 Å) than it was determined from an as-synthesized crystal by X-ray crystallography (5.2 Å).[3] **IFP-4** contains flexible ethyl groups. The effective channel diameter of 1.7 Å for **IFP-4** (Scheme 1) is calculated[2] and is only based on the conformation of the ethyl group at the energy minimum. Recently, Henke and Fischer showed that flexible methoxyethoxy groups in a honeycomb-like zinc–dicarboxylate–bipyridine framework act as molecular gates for guest molecules and allow highly selective sorption of CO_2 over CH_4.[16] The ethyl groups in **IFP-4** have also the potential to function as molecular gates for guest molecules. CO_2 can fill the whole pore volume of the porous material **IFP-1** to **IFP-6** at 273 K. By assuming that the adsorbate is in the liquid-like state at the saturation regime of the isotherms, one can apply the Gurvich rule (here at $p/p_0 = 0.5$) and the Dubinin–Radushkevich method for estimation of the pore volume.[17] The calculated values of the BET surface area can then be slightly different from values given in ref. 2, because of the difference in applied methods.

4.2 Pure gas adsorption

In Fig. 1 and 2, all CO_2 and CH_4 adsorption isotherms on **IFP** materials **IFP-1** to **IFP-6** are shown. For CH_4 no surface excess maximum was found until 5 MPa, whereas for CO_2 in some cases a surface excess maximum could be indicated. This is due to the fact that the adsorbed phase of CO_2 is at 273 K more compressible than the adsorbed phase of CH_4.[15a] At higher pressures a maximum for CH_4 can be observed, as shown in ref. 2. Hence for fitting the CO_2 adsorption isotherm all points were used before the maximum in surface excess was reached. All isotherms were then well described by the Tòth isotherm equation. An overview of fitting parameters is given in Table 2 and 3 including the average relative derivations. These values are quite

Table 1 Textural properties of **IFP** materials calculated from the CO_2 adsorption isotherm at 273 K

		Pore volume[17]	
	BET surface area[15]	Gurvich rule	DR method
Material	A_{BET}/m^2 g^{-1}	V_{Pore}/cm^3 g^{-1}	V_{Pore}/cm^3 g^{-1}
IFP-1	1068	0.31	0.32
IFP-2	940	0.26	0.28
IFP-3	622	0.18	0.18
IFP-4	674	0.22	0.23
IFP-5	574	0.18	0.18
IFP-6	985	0.27	0.28

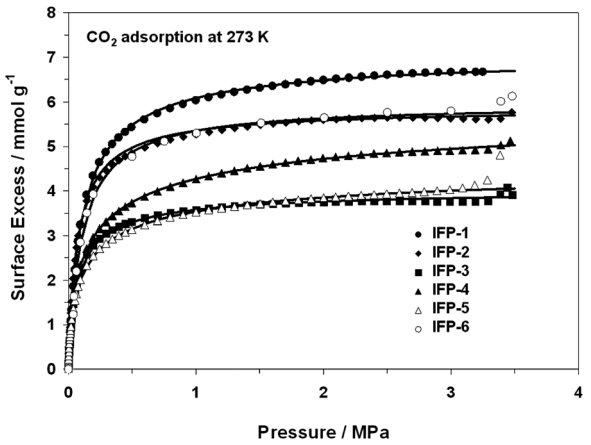

Fig. 1 CO_2 pure gas isotherms for **IFP-1–IFP-6**.

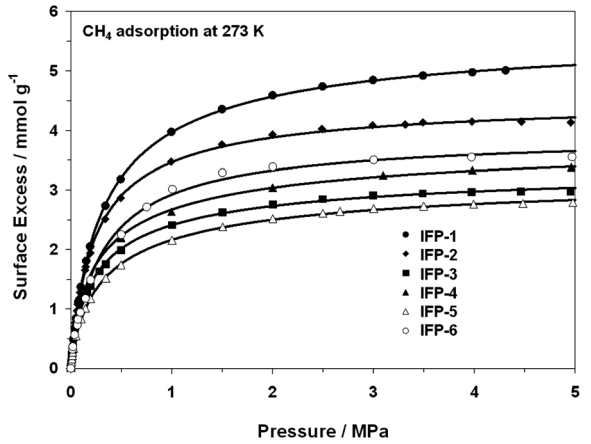

Fig. 2 CH_4 pure gas isotherms for **IFP-1–IFP-6**.

Table 2 Tòth isotherm model parameters for CO_2 adsorption isotherms and Henry's law constants for **IFP** materials at 273 K

CO_2 adsorption at 273 K					
Tòth parameter	$n^{\sigma}{}_{\infty}$/ mmol g^{-1}	b/MPa^{-1}	t	H/ mmol g^{-1} MPa^{-1}	$\bar{\Delta}n^{\sigma}$ (%)
IFP-1	7.077	11.64	0.824	82.37	1.63
IFP-2	5.885	15.74	0.886	92.60	2.67
IFP-3	4.077	22.56	0.735	91.99	3.49
IFP-4	6.329	35.03	0.457	221.71	0.57
IFP-5	4.770	31.67	0.517	151.09	2.27
IFP-6	5.962	9.79	0.966	58.37	4.12

low and indicate the good match between the experimental and modeled data.

As can be seen by comparing the isotherms in Fig. 1 and 2, CO_2 adsorption is preferred over CH_4 adsorption at low pressures and at high pressures by all **IFP** materials. At low pressures it is also indicated by the Henry's law constants given in Tables 2 and 3. The preference of CO_2 uptake is firstly due to the fact that CO_2 is more polarizable than CH_4 and therefore allows a stronger interaction with the surfaces of the **IFP**s. In addition, CO_2 consists of a quadrupole, whereas CH_4 is nonpolar.

Table 3 Tòth isotherm model parameters for CH_4 adsorption isotherms and Henry's law constants for **IFP** materials at 273 K

CH_4 adsorption at 273 K					
Tòth parameter	$n^{\sigma}{}_{\infty}$/ mmol g^{-1}	b/MPa^{-1}	t	H/ mmol g^{-1} MPa^{-1}	$\bar{\Delta}n^{\sigma}$ (%)
IFP-1	5.707	3.97	0.795	22.63	2.48
IFP-2	4.565	5.12	0.831	23.38	1.69
IFP-3	3.487	6.95	0.661	24.24	2.53
IFP-4	3.966	7.49	0.628	29.69	2.38
IFP-5	3.336	5.19	0.664	17.32	1.94
IFP-6	3.957	3.70	0.893	14.64	6.99

At higher pressures, the adsorbed amount of CO_2 is higher than that for CH_4, because CO_2 is below its bulk critical temperature (T_{C,CO_2} = 304.15 K), whereas CH_4 (T_{C,CH_4} = 190.55 K) is supercritical.

4.3 Mixed gas adsorption

In order to assess the separation potential and to classify the isoreticular series of **IFPs**, binary adsorption of nearly equimolar mixture of CO_2 and CH_4 was measured at 273 K and 0.1 MPa for each **IFP** material by a volumetric–chromatographic method. Additionally, binary adsorption was predicted using the IAST in comparison with the pure gas adsorption Tòth isotherm model for spreading pressure calculations. For all **IFP** materials the indicating spreading pressure diagram can be found in the ESI (Fig. S1–S6†). The partial molar loadings are given in Fig. 3a–f. In all cases the IAST + Tóth isotherm model predicts very well the mixture adsorbed amount, so that one can obtain an ideality of the adsorbed phase. The calculated relative derivations between experimental data and IAST prediction are given in Table 4, which differ slightly between **IFP** materials. For **IFP-6** the derivations are higher than in the case of the other **IFP** materials affected by the very low kinetic to reach adsorption equilibria. In that case more than 60 hours equilibrium time was chosen for measurement of binary mixtures.

The ideality of the adsorbed phase can also be seen in Fig. 4 (McCabe–Thiele diagrams), where the adsorbed phase molar fraction x_{CO_2} is plotted against the gas phase molar fraction y_{CO_2}. From such plots it is obvious that the adsorption of CO_2 is preferred over CH_4 adsorption for **IFPs** over the whole gas phase composition. If the IAST predicts the x–y distribution in a good manner, then the selectivity should be as well, which can be seen in Fig. 4, where the selectivities at 0.1 MPa and 273 K calculated from IAST are compared to experimental data.

It is obvious that for **IFP-1**, **IFP-2**, **IFP-3** and **IFP-6** the selectivities with α_{CO_2/CH_4} around 4–5 are lower than for **IFP-4** (around 6) and **IFP-5** (around 7.5) (Fig. 5). As already mentioned **IFP-4** consists of an open void space of 1.7 Å (without solvent or gas molecules in the void space) and ethyl groups from the ligand on the edge of these voids. Incoming gas molecules have to widen the void space by changing conformation of the ethyl groups arranged on the C1-atom of the imidazole ring. Because of the lower kinetic diameter of CO_2 (3.3 Å) in comparison to CH_4 (3.8 Å), the twist of the ethyl groups for incoming CO_2 has to be smaller as it has to be for CH_4.

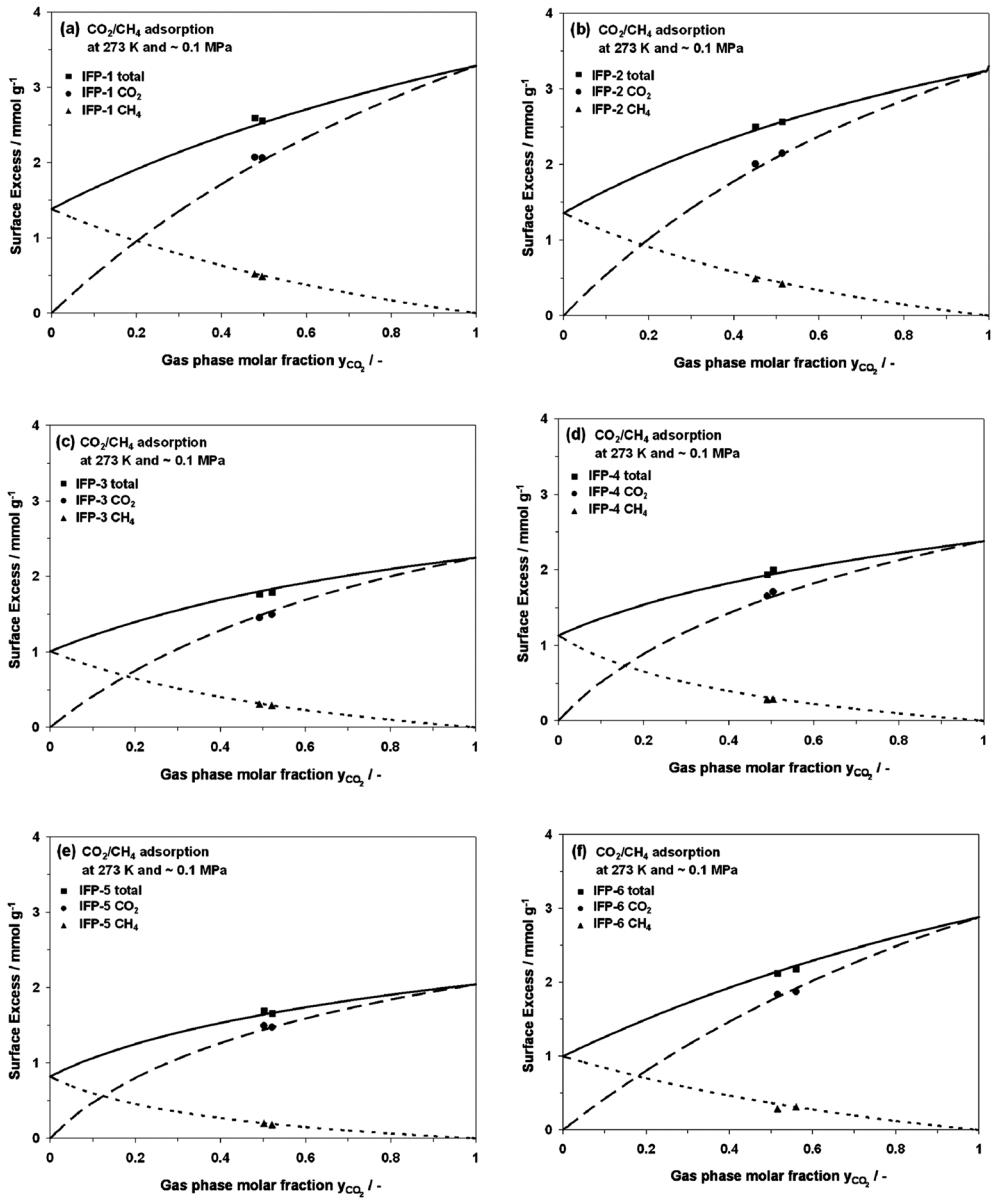

Fig. 3 (a–f) Partial molar loadings of CO_2 and CH_4 on (a) **IFP-1**, (b) **IFP-2**, (c) **IFP-3**, (d) **IFP-4**, (e) **IFP-5**, and (f) **IFP-6**.

Table 4 Binary adsorption of CO_2/CH_4 on **IFP** materials at 273 K and deviation between experimental data and prediction by IAST; adsorption selectivities for CO_2/CH_4 on **IFP** materials at 273 K

Material	p/MPa	y_{CO_2}	x_{CO_2}	Δx_{CO_2} (%)	Equilibrium time/h	$n^{\sigma}_{CO_2}$/ mmol g^{-1}	$\Delta n^{\sigma}_{CO_2}$ (%)	n^{σ}_{total}/ mmol g^{-1}	$\Delta n^{\sigma}_{total}$ (%)	Ideal selectivity from Henry's law constants	Experimental selectivity α_{CO_2/CH_4}
IFP-1	0.1017	0.478	0.799	1.12	22	2.074	3.98	2.594	2.89	3.64	4.35
	0.0991	0.496	0.807	0.51	46	2.065	2.14	2.558	1.64		4.26
IFP-2	0.0948	0.451	0.804	0.98	20	2.010	4.05	2.500	3.10	3.96	5.00
	0.0970	0.514	0.836	0.10	4	2.150	0.26	2.571	0.16		4.82
IFP-3	0.0989	0.492	0.826	0.08	20	1.455	1.65	1.762	1.58	3.79	4.89
	0.1009	0.521	0.838	0.53	6	1.500	3.23	1.790	2.69		4.76
IFP-4	0.0969	0.490	0.853	1.49	22	1.651	3.20	1.935	1.73	7.47	6.04
	0.1016	0.504	0.854	0.77	6	1.709	3.03	2.000	2.27		5.77
IFP-5	0.0999	0.502	0.883	0.58	19	1.494	3.50	1.692	2.94	8.72	7.52
	0.1008	0.521	0.890	0.32	4	1.475	0.27	1.657	0.63		7.44
IFP-6	0.1050	0.560	0.860	0.59	65	1.873	5.63	2.179	5.01	3.99	4.81
	0.1038	0.515	0.866	2.90	69	1.836	0.32	2.122	3.31		6.06

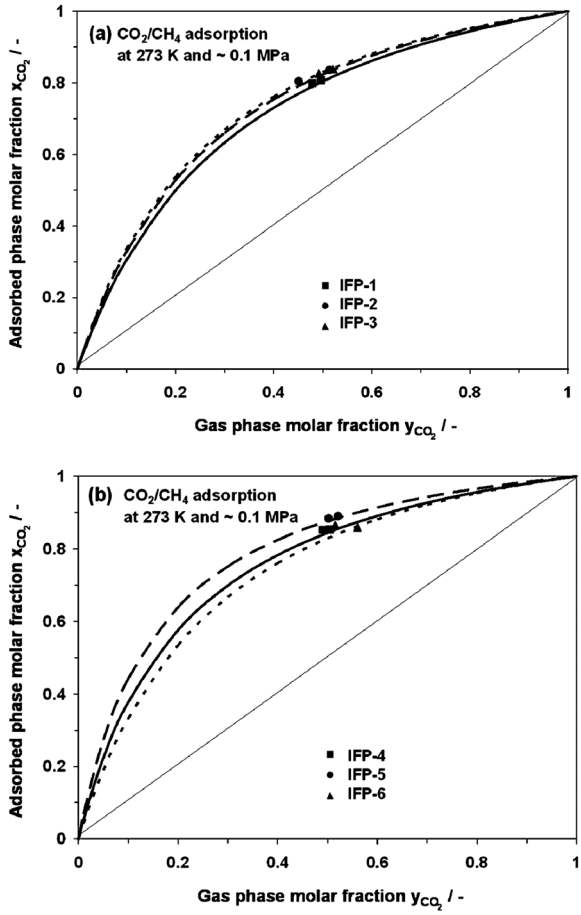

Fig. 4 (a) McCabe–Thiele diagram for adsorption of CO_2/CH_4 on **IFP-1** (solid line, IAST + Tòth isotherm model), **IFP-2** (dashed line, IAST + Tòth isotherm model) and **IFP-3** (dotted line, IAST + Tòth isotherm model) and (b) on **IFP-4** (solid line, IAST + Tòth isotherm model), **IFP-5** (dashed line, IAST + Tòth isotherm model) and **IFP-6** (dotted line, IAST + Tòth isotherm model).

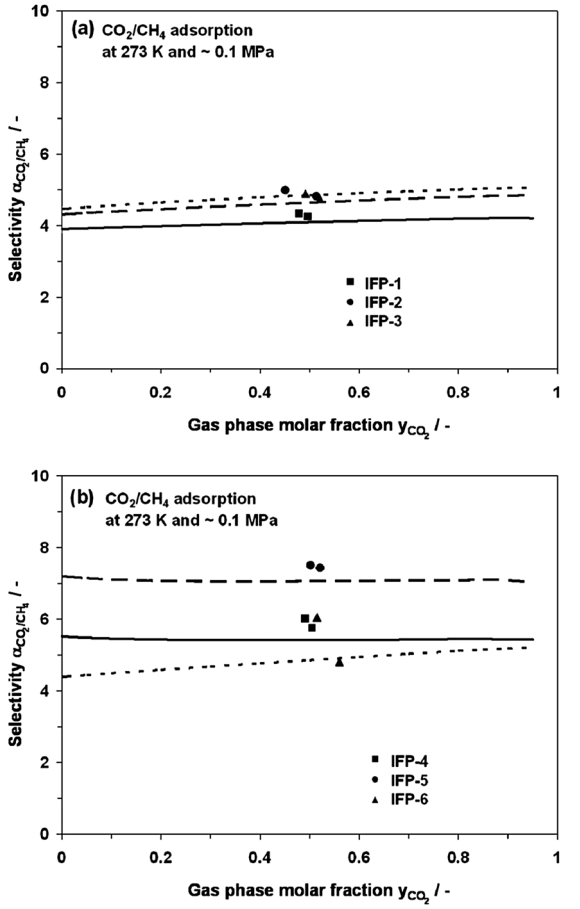

Fig. 5 (a) Adsorption selectivity α_{CO_2/CH_4} on **IFP-1** (solid line, IAST + Tòth isotherm model), **IFP-2** (dashed line, IAST + Tòth isotherm model) and **IFP-3** (dotted line, IAST + Tòth isotherm model) and (b) on **IFP-4** (solid line, IAST + Tòth isotherm model), **IFP-5** (dashed line, IAST + Tòth isotherm model) and **IFP-6** (dotted line, IAST + Tòth isotherm model).

Therefore, **IFP-4** shows higher selectivity compared to **IFP-1** to **IFP-3** and **IFP-6**. In contrast, **IFP-5** has the highest selectivity in this series of **IFPs** with α_{CO_2/CH_4} around 7.5 at 273 K and 0.1 MPa. That might be due to the presence of the unsaturated metal site of the paramagnetic Co centre. We assume that the Co centres in **IFP-5** have a higher potential to polarize CO_2 molecules than the Zn and Cd centres in the other **IFP**s.

In Table 4, the selectivities obtained from experimental data are shown. Such values differ from ideal selectivity due to the Henry's law region of pure gas isotherms (Table 2 and 3). However, the trend between all **IFP** materials is the same.

However, with the preferred adsorption of CO_2 over CH_4, this series of **IFPs** and especially **IFP-5** could be a promising candidate for biogas purification or for CO_2 capture from CH_4-based gas mixtures on the equilibrium effect. In more detail, state-of-the-art adsorbents like activated carbons show slightly lower selectivities for CO_2 within a range of $\alpha_{CO_2/CH_4} = 2–6$[18–21] than in the case for **IFP-5**. Whereas hydrophilic zeolites show higher affinity towards H_2O and CO_2 resulting in a higher selectivity for the separation of CO_2 from a CO_2/CH_4 mixture. Zeolites have at a slightly higher temperature regime (273 K < T > 333 K) selectivities of about $\alpha_{CO_2/CH_4} > 6$,[18,22–26] and in addition the disadvantage that the CO_2 adsorption capacity depends on the value of preadsorbed H_2O. Thus, the reactivation of such materials might be problematic. The selectivity of **IFP-5** is just higher than for porous clays ($\alpha_{CO_2/CH_4} = 2–3$).[27] Comparing to MOFs, the equilibrium selectivities of **IFP-4** and **IFP-5** are in the same order of magnitude as in the case of HKUST-1 ($\alpha_{CO_2/CH_4} =$ 5–7 at 0.1 MPa and 303 K),[28] MIL-53-Al ($\alpha_{CO_2/CH_4} = 7$ below 0.5 MPa and 303 K),[29] MIL-53-Cr ($\alpha_{CO_2/CH_4} = 3–15$ at different pressures and 303 K)[30] and MIL-101-Cr ($\alpha_{CO_2/CH_4} = 3.6–7.5$ at different pressures and 298 K),[31] but lower than for amine-functionalized MIL-101-Al ($\alpha_{CO_2/CH_4} = 30–50$ at 298 K).[31]

Eventually, **IFP-4** and **IFP-6** could be also promising candidates for the exploitation of a kinetic separation. Regarding their small void space, both materials exhibit a molecular sieving effect, which will be studied further.

5 Conclusions

We carried out pure gas and binary gas adsorption measurements of CO_2 and CH_4 on an isoreticular series of **IFP** materials

at 273 K. The experimental pure gas isotherms were well described by the Tòth isotherm equation. Binary adsorption data were further predicted with IAST, which are in excellent agreement with experimental data.

From these data, we could show further that **IFP** materials can keep up with selectivities of other well known MOF materials (*e.g.* HKUST-1 and different MIL structures). The most promising CO_2/CH_4 gas selectivity in the series of **IFP** materials shows **IFP-4** and **IFP-5**. The behaviour of **IFP-5** could be explainable *via* enhancement of the electronic interaction between CO_2 and the unsaturated metal site of the paramagnetic Co centre. **IFP-4** is the material with the smallest pore diameter when the pores are empty, they should be too small for incoming CO_2 or CH_4. But relatively mobile ethyl groups in 2-position of the linkers can widen the pores by incoming gas molecules at relatively high temperatures (here 273 K). Because of smaller CO_2 molecules in comparison to CH_4 incoming CO_2 has to widen the pores to a smaller extent. This effect in addition to the bigger interaction of CO_2 *via* its quadrupole and the free exposed zinc centre, the CO_2 uptake is strongly preferred over CH_4 uptake in this case.

Future studies will deal with the kinetic gas separation potential of **IFP-4** and **IFP-6**, *e.g.* CH_4/N_2 or Ar/O_2 should be examined. Furthermore the influence of competing, polar water molecules on the capacity and selectivity of CO_2 in **IFPs** will be tested.

Acknowledgements

We thank the Deutsche Forschungsgemeinschaft (DFG SPP 1362—Poröse metallorganische Gerüstverbindungen, STA 428/17-1 and HO 1706/6-2) for financial support.

Notes and references

1 F. Debatin, A. Thomas, A. Kelling, N. Hedin, Z. Bacsik, I. Senkovska, S. Kaskel, M. Junginger, H. Müller, U. Schilde, C. Jäger, A. Friedrich and H.-J. Holdt, *Angew. Chem.*, 2010, **122**, 1280; *Angew. Chem., Int. Ed.*, 2010, **49**, 1258.
2 F. Debatin, K. Behrens, I. A. Baburin, I. Senkovska, S. Kaskel, A. Thomas, J. Schmidt, J. Weber, A. Kelling, S. Leoni, G. Seifert, C. Jäger, J. Möllmer, A. Möller, R. Staudt, U. Schilde, A. Friedrich and H.-J. Holdt, *Chem. Eur. J.*, 2012, submitted.
3 S. S. Mondal, F. Debatin, I. Senkovska, S. Kaskel, A. Thomas, J. Schmidt, J. Weber, A. Kelling, C. Jäger, U. Schilde, A. Friedrich and H.-J. Holdt, in preparation.
4 (*a*) H. Hayashi, A. P. Coté, H. Furukawa, M. O'Keeffe and O. M. Yaghi, *Nat. Mater.*, 2007, **6**, 501; (*b*) A. Phan, C. J. Doonan, F. J. Uribe-Romo, C. B. Knobler, M. O'Keeffe and O. M. Yaghi, *Acc. Chem. Res.*, 2010, **43**, 58.
5 J. U. Keller and R. Staudt, *Gas Adsorption Equilibria—Experimental Methods and Adsorption Isotherms*, Springer, New York, USA, 2004.
6 (*a*) R. Span and W. Wagner, *J. Phys. Chem. Ref. Data*, 1996, **25**, 1509; (*b*) R. D. McCarty, *Adv. Cryog. Eng.*, 1990, **35**, 1465; (*c*) U. Setzmann and W. Wagner, *J. Phys. Chem. Ref. Data*, 1991, **20**, 1061.
7 O. Kunz, R. Klimeck, W. Wagner and M. Jaeschke, *GERG Technical Monograph 2*, VDI, 1988.
8 J. Möllmer, A. Möller, C. Patzschke, K. Stein, D. Lässig, J. Lincke, R. Gläser, H. Krautscheid and R. Staudt, *J. Mater. Chem.*, submitted.
9 D. D. Do, *Adsorption Analysis: Equilibria and Kinetics*, Imperial College Press, vol.2, 1998.
10 I. Langmuir, *J. Am. Chem. Soc.*, 1918, **40**, 1361.
11 J. Tòth, *Adv. Colloid Interface Sci.*, 1995, **55**, 1.
12 A. L. Myers and J. M. Prausnitz, *AIChE J.*, 1965, **11**, 121.
13 O. Talu and A. L. Myers, *AIChE J.*, 1988, **34**, 1887.
14 O. Talu, *Chem. Ing. Tech.*, 2011, **83**, 67.
15 (*a*) J. Moellmer, E. B. Celer, R. Luebke, A. J. Cairns, R. Staudt, M. Eddaoudi and M. Thommes, *Microporous Mesoporous Mater.*, 2010, **129**, 345; (*b*) ISO/FDIS 9277:2010.
16 S. Henke and R. A. Fischer, *J. Am. Chem. Soc.*, 2011, **133**, 2064.
17 S. Lowell, J. Shields, M. A. Thomas and M. Thommes, *Characterization of Porous Solids and Powders: Surface Area, Pore Size and Density*, Springer, The Netherlands, 2004.
18 W. Sievers and A. Mersmann, *Chem. Eng. Technol.*, 1994, **17**, 325.
19 E. Buss, *Gas Sep. Purif.*, 1995, **9**, 189.
20 F. Dreisbach, R. Staudt and J. U. Keller, *Adsorption*, 1999, **5**, 215.
21 V. Goetz, O. Pupier and A. Guillot, *Adsorption*, 2006, **12**, 55.
22 P. D. Rolniak and R. Kobayashi, *AIChE J.*, 1980, **26**, 616.
23 P. J. E. Harlick and F. H. Tezel, *Sep. Sci. Technol.*, 2002, **37**, 33.
24 P. J. E. Harlick and F. H. Tezel, *Sep. Purif. Technol.*, 2003, **33**, 199.
25 S. Cavenati, C. A. Grande and A. E. Rodrigues, *J. Chem. Eng. Data*, 2004, **49**, 1095.
26 N. Heymans, B. Alban, S. Moreau and G. DeWeireld, *Chem. Eng. Sci.*, 2011, **66**, 3850.
27 J. Pires, M. Bestilleiro, M. Pinto and A. Gil, *Sep. Purif. Technol.*, 2008, **61**, 161.
28 L. Hamon, E. Jolimaitre and G. D. Pirngruber, *Ind. Eng. Chem. Res.*, 2010, **49**, 7497.
29 V. Finsy, L. Ma, L. Alaerts, D. E. De Vos, G. V. Baron and J. F. M. Denayer, *Microporous Mesoporous Mater.*, 2009, **120**, 221.
30 L. Hamon, P. L. Llewellyn, T. Devic, A. Ghoufi, G. Clet, V. Guillerm, G. D. Pirngruber, G. Maurin, C. Serre, G. Driver, W. Van Beek, E. Jolimaitre, A. Vimont, M. Daturi and G. Ferey, *J. Am. Chem. Soc.*, 2009, **131**, 17490.
31 P. Serra-Crespo, E. V. Ramos-Fernandez, J. Gascon and F. Kapteijn, *Chem. Mater.*, 2011, **23**, 2565.